Article

Theoretical Analysis of an Integrated, CPVT Membrane Distillation System for Cooling, Heating, Power and Seawater Desalination

Abeer Abdullah Al Anazi [1], Mohammed I. Alghamdi [2], Abdeljelil Chammam [3], Mustafa Salam Kadhm [4], Ibrahim H. Al-Kharsan [5] and Reza Alayi [6,7,*]

1. Department Mechanical Engineering, University Australian (AU), Kuwait 13015, Kuwait
2. Department Computer Engineering and Computer Sciences, Al-Baha University, Al-Baha 65528, Saudi Arabia
3. Department of Electrical Engineering, College of Engineering, Prince Sattam Bin Abdulaziz University, Al-Kharj 11942, Saudi Arabia
4. Department of Computer Technology Engineering, College of Information Technology, Imam Ja'afar Al-Sadiq University, Baghdad 66002, Iraq
5. Computer Technical Engineering Department, College of Technical Engineering, The Islamic University, Najaf 338-0826, Iraq
6. Department of Mechanics, Germi Branch, Islamic Azad University, Germi 1477893855, Iran
7. Energy Research Centre, Shahrekord Branch, Islamic Azad University, Shahrekord 88137-33395, Iran
* Correspondence: reza_alayi@iaugermi.ac.ir

Abstract: Compared to a photovoltaic array, a photovoltaic/thermal concentrator module can produce thermal power for various productions in downstream cycles in addition to electrical energy. In this study, the system for the combined production of electricity, heat and cooling based on a photovoltaic/thermal concentrator has been evaluated. In this triple production system, a lithium bromide-water absorption chiller with a cooling capacity of 5 kW was used. In the organic Rankine power generation cycle, the annual exergy rate of the incoming stream was almost 48 MWh, the annual production exergy rate was about 54.4 MWh and the annual exergy destruction rate was ~43.1 MWh. According to the results, the freshwater production rate of the desalination plant was approximately 56.7 m^3/year; the lowest month was 3.8 m^3 in November.

Keywords: concentration photovoltaic/thermal; organic Rankine cycle; absorption refrigeration; membrane distillation; exergy

1. Introduction

Energy consumption is increasing due to the increase in population, the expansion of cities and the improvement in the quality of life. On the other hand, the rapid consumption of energy has led to the uncontrolled release of carbon dioxide and other greenhouse gases, as well as global warming. In addition, the water crisis is one of the problems facing mankind in the last century, along with the energy crisis. Due to the increasing growth of energy consumption, the increase in greenhouse gases and the water crisis, the tendency to use renewable energy has increased, and among renewable energies, solar energy has received more attention. One of the most important applications of solar energy is its conversion into electrical energy using photovoltaic cells. Among the different technologies of photovoltaic cells, concentrating photovoltaic cells have attracted the attention of many large companies in the field of photovoltaics as a suitable alternative to conventional photovoltaic cells. Increasing the temperature of photovoltaic systems reduces their performance, so heat removal from photovoltaic systems is desirable to increase their efficiency. Due to the high thermal power produced in these systems due to the concentration of radiation on photovoltaic cells, the waste heat from photovoltaic modules is used to produce hot water, for power generation using the rockin' cycle and for freshwater production using water

softeners. Membrane distillation, cooling production using absorption refrigeration systems and also heating have been considered. The combination of photovoltaic systems with the organic Rankine cycle, while reducing the operating temperature of the photovoltaic system, also leads to the production of additional electricity. In this combined system, there is an optimal temperature in which the total electricity produced by the combined system is maximum. In the study carried out by Meltams and Roshan Del [1], a combined and modified photovoltaic system using a Rankine cycle thermal concentrator was simulated and the efficiency temperature of the photovoltaic system was determined for different efficiencies of this system. This research showed that increasing the nominal efficiency of the photovoltaic system leads to choosing a lower temperature as its optimal temperature. Rahbar et al. [2], used a combined nanofluid-based thermal concentrator photovoltaic system with the organic Rankine cycle for heat recovery and also used r233z working fluid in the organic Rankine cycle. In this study, they compared the aforementioned combined system with the combined thermal concentrator system based on the working fluid and found that the electrical, thermal and total efficiency were 1.85%, 3.3% and 5.1%, respectively, and the values of these parameters increased compared to the concentrator combined system with water as the working fluid and the total efficiency increased by 2.71% compared to the concentrator combined system. Albaik et al. [3], developed a solar-driven adsorption-ORC system, which was proposed by considering different homogenizer types (reflective, refractive and coated refractive) in the CPV/T. The cells operated at a higher optical performance and outlet water temperature compared to the literature. The results of each subsystem in the integrated system were also experimentally validated. An MJSC that can be operated up to a temperature of 110 °C was used in order to maximize the cooling water temperature that can be extracted as a thermal power from the cells.

Noorollahi et al. [4], in their study aimed to investigate the technical and economic aspects of a hybrid concentrated photovoltaic thermal/organic Rankine cycle (CPV/T-ORC) system for the simultaneous generation of power and heat in the summer and winter seasons. In another study, a new combined photovoltaic concentrator/membrane desalination system was proposed for the simultaneous production of sweet water electricity by Elminshawi et al. [5]. The results showed that the combined system was able to convert 83% of the Sun's radiation into useful output and improve the production power of the concentrating photovoltaic joule by 26.6% compared to the module without a cooling system. In the study conducted by Heng et al. [6], a combined photovoltaic thermal concentrator system with a low concentration coefficient/water-lithium bromide absorption refrigeration system was investigated. In this study, experiments were carried out to investigate the effect of the parameters for the inlet hot water temperature, cooling water mass flow rate and cooling water mass flow rate on the performance coefficient of the absorption refrigeration system, and relations were presented to calculate the performance coefficient and cooling coefficient according to the above parameters. Buonomano et al. [7], presented a new dynamic simulation model for heating and cooling systems with concentrator photovoltaic and flat plate collectors in the Matlab @R2021b software. They investigated the energy, economic and environmental aspects of the system based on absorption chiller technologies. The analysis was focused on office and residential buildings in different European climate zones. Mohammad Rabia et al. [8], performed thermal analysis of a combined photovoltaic heat concentrator system with a high concentration coefficient/membrane distillation water desalination for the simultaneous production of power and freshwater in coastal areas. The results showed that in sunlight with a concentration ratio of 1000, the cooling water flow should be more than 150 g/min so that the maximum temperature of the photovoltaic cell does not exceed 349 K. In these conditions, the electrical and thermal power produced was 177 and 308 watts, respectively. Moalleman et al. [9], simulated the performance of the simultaneous heating, cooling and power generation system based on the thermal concentrator photovoltaic system with the linear Fresnel collector in the TRNSYS18 software. In this triple production system, a lithium bromide-water absorption chiller with a cooling capacity of 5 kW was used. They compared the concentrator photovoltaic system with

a conventional photovoltaic system and it was concluded that the conventional system cannot provide the thermal energy required for cooling. Due to the high production thermal power of the concentrator photovoltaic system and also the high temperature of the cooling fluid output from the system, this system can be used for the simultaneous production of power, cooling and freshwater. This issue encouraged the authors to analyze the combined photovoltaic system made up of a heat concentrator, organic Rankine power generation cycle, absorption cooling and membrane distillation desalination from the point of view of energy and exergy in the transient state, a study that has not been conducted so far. In the following, the combined description system and the governing equations from the point of view of energy and exergy for the system are presented and, at the end, the results from the simulation of this system are presented.

2. Materials and Methods

2.1. System Description

As shown in Figure 1, the desired hybrid system consists of a thermal concentrator photovoltaic module, a storage tank, an organic Rankine cycle, an absorption cooling cycle and a membrane distillation desalination plant. In the proposed system, the thermal concentrator photovoltaic module (CPV/T) is able to produce thermal and electrical energies. The desired module is based on a parabolic trough collector. The thermal energy obtained from this module is stored in a storage tank to be directed to the organic Rankine cycle (ORC) if needed. The organic Rankine cycle produces electrical energy under a Rankine process using an organic fluid. The waste heat from the ORC is directed to an absorption cooling cycle and then to a membrane distillation desalination plant in two stages to produce cooling load and freshwater, respectively. Therefore, the proposed hybrid energy system can generate electric power, cooling and heating loads, and freshwater. The Matlab and EES Pro 10.561 software are employed to simulate the offered energy system.

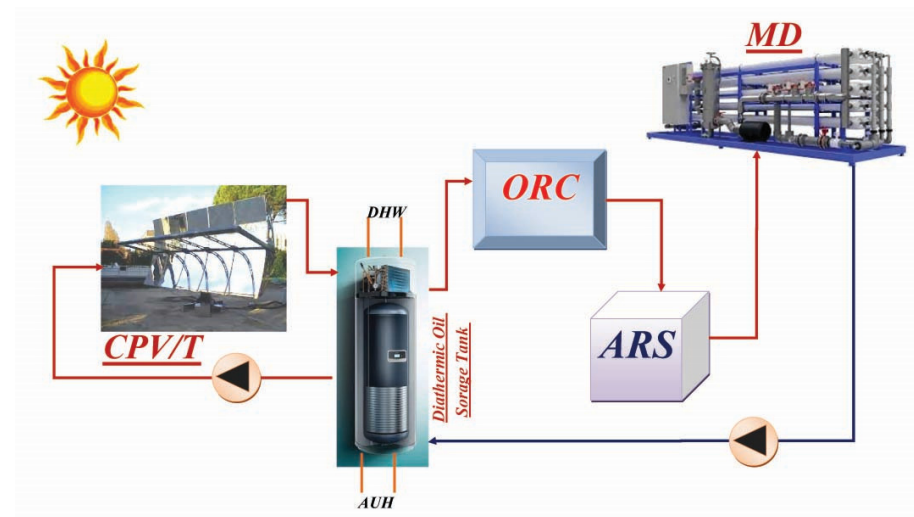In the following, the modeling of the different parts of the combined system are discussed.

Figure 1. Schematic diagram of the proposed hybrid energy system.

2.2. Governing Equations

In this section, the energy and exergy equations for each part of the described combined system are presented.

2.2.1. Concentration Photovoltaic/Thermal

Energy Equations

Since multi-connection cells are used in concentrator photovoltaic panels, the electrical performance of these types of panels is affected by a factor called the thermal factor, which

is used to calculate this factor using Equation (1). The maximum power temperature coefficient is in the functional focus, which is equal to 0.0012 [10]:

$$TF = 1 - \gamma \times (T_C - T_{STC}) \tag{1}$$

To calculate the temperature of the T_C cells, Equation (2) is used, in which the special thermal coefficient of the concentrator is equal to 6% [10]:

$$T_C = T_a + a \times I_{bT} \tag{2}$$

In Equation (2), I_{bT} is the direct solar radiation. The ideal electrical energy produced by each multi-junction solar cell can be calculated using Equation (3) [10]:

$$P_{id} = I_{bT} \times A_{cell} \times X \times \eta_{cell} \tag{3}$$

In this regard, the efficiency of the cell in standard conditions is calculated by Equation (4), and the area of each solar cell is in square meters, and the effective x-axis is calculated using Equation (5) [11]:

$$\eta_{cell} = 0.298 + 0.014 \times LnC + (-0.000715 + 0.0000697 \times LnC) \times (T_c - 25\,°C) \tag{4}$$

$$X = \eta_{Opt} * C \tag{5}$$

In Equations (4) and (5), C is the geometric concentration coefficient of the concentrator system, which is obtained from Equation (6), and subscript Opt refers to the optical efficiency of the concentrator, which can be extracted from the catalog of the concentrator. The value of this parameter is equal to 0.85 [11]:

$$C = \frac{A_{aperture}}{A_{cell}} \tag{6}$$

Note that the desired thermal concentrator photovoltaic module is based on a parabolic trough collector. The schematic diagram of a parabolic trough collector is portrayed in Figure 2. A parabolic trough collector is a linear focus solar collector, basically composed of a parabolic trough shaped concentrator that reflects direct solar radiation onto a receiver or absorber tube. The concentration ratio of these collectors is in the range of 10–85. (The energy, exergy, environmental and economic comparison of various solar thermal systems using water and Thermia Oil B base fluids, and CuO and Al_2O_3 nanofluids.)
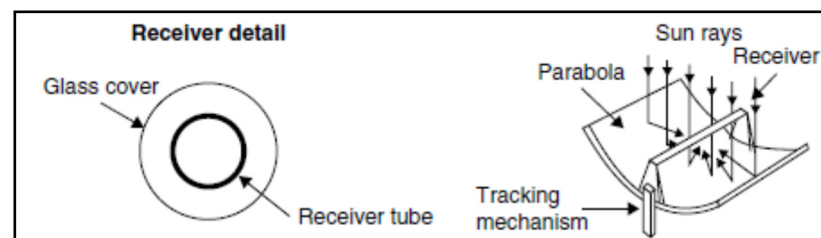

Figure 2. Schematic diagram of a parabolic trough collector.

In Equation (6), $A_{aperture}$ is the area of the opening. By combining Equations (1)–(6), the electrical energy produced by each cell is obtained as follows [11]:

$$P = I_{bT} \times A_{cell} \times \eta_{cell} \times \eta_{Opt} \times C \times TF \times SF \tag{7}$$

To calculate the real energy of this system, the power of the pump, the detector and the efficiency of the inverter must be reduced from this value, which is called parasitic loss and is calculated using Equation (8):

$$P_{par} = 0.023 \times A_{cell} \times C \times \eta_{cell} \times I_{bT} \tag{8}$$

Finally, the real electrical energy can be obtained as follows:

$$P_{real} = P - P_{par} \tag{9}$$

Equation (10) estimates the ideal thermal energy of the module [11]:

$$Q_{th.id} = \left(1 - \eta_{pv}\right) \times \eta_{opt} \times C \times (I_{bT} \times F) \times A_{cell} \times n_{cell} \tag{10}$$

In Equation (10), according to the non-ideal detector system, the F factor applied is equal to 0.9. The overall efficiency of the concentrator photovoltaic system and the thermal coefficient of the power can be calculated from the following relations [11]:

$$\eta_{pv} = \eta_{cell} \times \eta_{mod} \times k_t \tag{11}$$

$$k_t = 1 + \sigma_t \times (T_c - 25) \tag{12}$$

In addition, the solar rays that reach the three junction cells have heat loss, which can be calculated according to Equation (13) [11]:

$$Q_{th,loss} = \left[h_c \times (T_c - T_a) + \varepsilon\sigma\left(T_c^4 - T_a^4\right)\right] \times A_{cell} \times n_{cell} \tag{13}$$

In this regard, the coefficient of heat transfer is different from one place to another. Now, the actual thermal energy produced can be calculated using Equation (14):

$$Q_{th,real} = Q_{th,id} - Q_{th,loss} \tag{14}$$

Exergy Equations

In Equation (15), the exergy of solar radiation is given [12].

$$EX_{sol} = A_{coll}G\left[1 + \frac{1}{3}\left(\frac{T_o}{T_{sun}}\right)^4 - \frac{4}{3}T\left(\frac{T_o}{T_{sun}}\right)\right] \tag{15}$$

Equation (16) shows the exergy difference between the output and input current of the solar collector.

$$EX_{coll} = \dot{m}_{coll}C\left[(T_{out} - T_{in}) - T_o \ln\left(\frac{T_{out}}{T_{in}}\right)\right] \tag{16}$$

The Equation (17) shows the exergy efficiency of the solar concentrator [12].

$$\psi = \frac{EX_{coll}}{EX_{sol}} \tag{17}$$

2.3. Rankine Cycle

Energy Equations

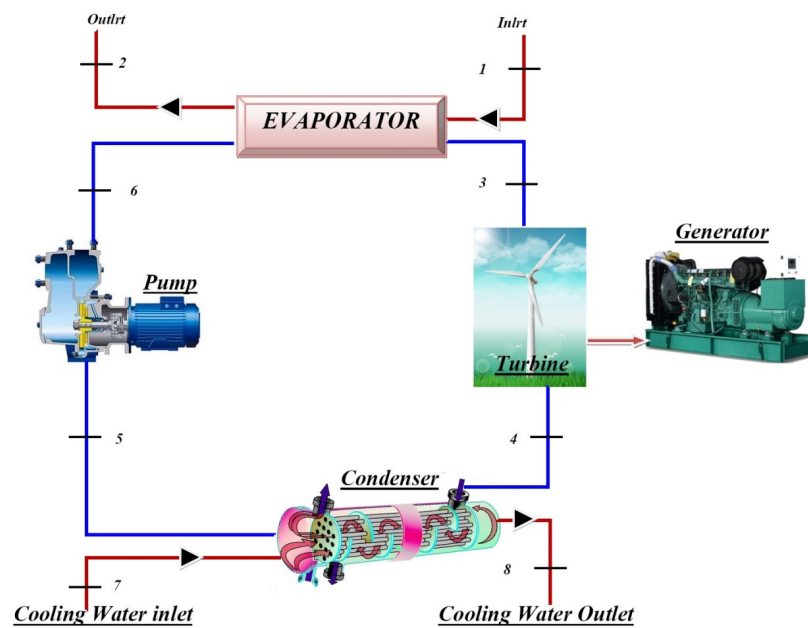Figure 3 shows a schematic of an organic Rankin cycle.

Figure 3. Schematic of the organic Rankine cycle.

The work produced in the turbine in this cycle is obtained from Equation (18) [13].

$$W_T = \dot{m}(h_3 - h_4) \tag{18}$$

The exergy efficiency of the evaporator and the condenser can be calculated by dividing the exergy obtained by the cold flow to the exergy supplied by the hot flow, according to Equations (19) and (20).

$$\eta_{ev} = \frac{\dot{m}_r(e_2 - e_6)}{\dot{m}_s(e_1 - e_2)} = 1 - \frac{\dot{I}_{ev}}{\dot{E}_1 - \dot{E}_2} \tag{19}$$

$$\eta_{con} = \frac{\dot{m}_w(e_8 - e_7)}{\dot{m}_r(e_4 - e_5)} = 1 - \frac{\dot{I}_{con}}{\dot{E}_4 - \dot{E}_5} \tag{20}$$

The exergy efficiency of the cycle is calculated from the ratio of the output network to the total exergy supplied, according to Equation (21).

$$\eta_{ex,cyc} = \frac{\dot{W}_{net,out}}{\dot{E}_{in}} = \frac{\dot{W}_{net,out}}{\dot{m}_s[h_1 - h_2 - T_o(s_1 - s_2)]} \tag{21}$$

The exergy destruction of the whole system can be calculated according to the Equation (22), and in fact, it is the sum of the exergy destruction of all the Sigel components [13].

$$\dot{I}_{cyc} = \dot{I}_{ev} + \dot{I}_T + \dot{I}_{con} + \dot{I}_{pump} \tag{22}$$

2.4. Absorption Cooling Cycle

2.4.1. Energy Equations

Figure 4 shows a schematic of a single effect absorption refrigeration system.
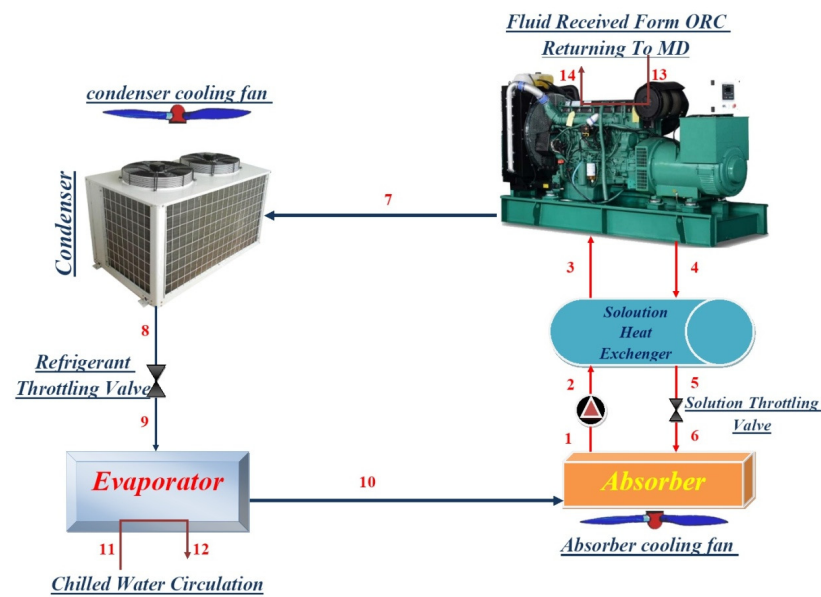
Figure 4. Schematic of a single effect absorption cooling cycle.

By completing the total mass conservation equation and the lithium bromide mass conservation equation in the absorber and using the concentrations obtained for the concentrated and dilute solution, the mass flow rate of the dilute solution entering and the concentrated solution leaving the absorber is obtained.

$$\dot{m}_1 = \dot{m}_6 + \dot{m}_{10} \tag{23}$$

$$\dot{m}_1 X_1 = \dot{m}_6 X_6 \tag{24}$$

In the above equation, X is the mass ratio of lithium bromide in a concentrated solution (a solution with a higher amount of water) and X_1 is the mass ratio of lithium bromide in a dilute solution (a solution with a lower amount of water). Using relations (25) and (26), the temperatures of points 3 and 5 are obtained.

$$T_3 = T_{abs} + E_L \frac{X_1 C_{p4}}{X_6 C_{p1}} \left(T_{gen} - T_{abs} \right) \tag{25}$$

$$T_5 = T_{gen} + E_L \left(T_{gen} - T_{abs} \right) \tag{26}$$

After obtaining the enthalpy of the refrigerant at point 7, using its temperature and pressure, the amount of heat produced in the condenser is obtained from Equation (27).

$$\dot{Q}_{con} = \dot{m}_7 (h_7 - h_8) \tag{27}$$

The required heat of the generator is obtained from the following equation:

$$\dot{Q}_{gen} = \dot{m}_7 h_7 + \dot{m}_4 h_4 - \dot{m}_3 h_3 \tag{28}$$

Also, the heat produced in the Bernese absorber is obtained from Equation (29).

$$\dot{Q}_{abs} = \dot{m}_{10} h_{10} + \dot{m}_6 h_6 - \dot{m}_1 h_1 \tag{29}$$

By obtaining the enthalpy of the solution at point 2, the required power of the pump is obtained from Equation (30).

$$Q_{pupmp} = \dot{m}_1(h_2 - h_1) \tag{30}$$

Finally, the coefficient of performance of the absorption chiller is calculated from Equation (31) [14].

$$COP = \frac{\dot{Q}_{eva}}{\dot{Q}_{gen} + W_{pump}} \tag{31}$$

2.4.2. Exergy Equations

In Table 1, the exergy balance equations for each part of the absorption chiller are given.

Table 1. Exergy balance equations for the absorption cooling cycle components.

Components	Equations
Generator	$EX_{dGe} = \dot{EX}_3 + \dot{EX}_{13} - \dot{EX}_4 - \dot{EX}_7 - \dot{EX}_{14}$
Evaporator	$EX_{d_{Eva}} = \dot{EX}_9 + \dot{EX}_{11} - \dot{EX}_{10} - \dot{EX}_{12}$
Condenser	$EX_{d_{Con}} = \dot{EX}_7 + \dot{EX}_8 - Q_{con}\left(1 - \frac{T_o}{T_{amb}}\right)$
Absorber	$EX_{d_{Abs}} = \dot{EX}_6 + \dot{EX}_{10} - \dot{EX}_8 - Q_{Abs}\left(1 - \frac{T_o}{T_{amb}}\right)$
Heat exchanger	$EX_{d_{Shx}} = \dot{EX}_4 + \dot{EX}_2 - \dot{EX}_5 - \dot{EX}_3$
Pump	$EX_{d_{Shx}} = \dot{EX}_1 + \dot{EX}_2 - W_{pump}$
Cooling system expansion valve	$EX_{d_{rev,v}} = \dot{EX}_8 + \dot{EX}_9$
Pressure relief valve	$EX_{d_{sev,v}} = \dot{EX}_5 + \dot{EX}_6$

2.5. Distillation System

2.5.1. Energy Equations

In this section, the distillation equations for the membrane distillation will be presented. Figure 5 is a schematic representation of a membrane distillation desalination system.
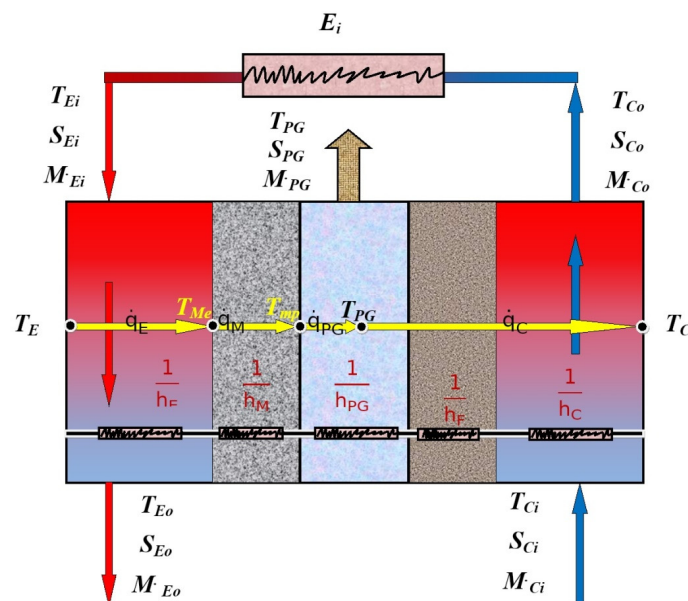

Figure 5. Schematic of a membrane distillation desalination system.

The transferred heat, thermal resistance and input and output parameters of each channel are shown in Figure 4. The first thermal resistance is the displacement thermal re-

sistance in the evaporator channel. The relation (32) shows the corresponding heat transfer.

$$\dot{Q}_E = h_E \left(\frac{T_{Ei} + T_{E0}}{2} - T_{Me} \right) \tag{32}$$

In this regard, the heat transfer coefficient in the evaporator channel is the temperature of the membrane surface in the evaporator channel. Heat (PM) is transferred in two ways, conduction and latent heat [15].

$$\dot{Q}_M = \frac{k_M}{\delta_M} \left(T_{Ms} - T_{Mp} \right) + j_p h_{fg} \tag{33}$$

In Equation (33), $h_{f,g}$ is the enthalpy of water evaporation and k_m, δ_M are the conductivity coefficient and membrane thickness, respectively. J_P is the mass transfer rate of permeated water (freshwater passing through the membrane) per unit area of the membrane. Also, T_{mp} is the temperature of the membrane surface in the distance of the infiltration flow. The rate of heat transfer in the distance of the infiltration flow is obtained using Equation (34):

$$\dot{Q}_{PG} = \frac{1}{\frac{\delta_{PG}}{2k_{PG}}} \left(T_{Mp} - T_{PG} \right) \tag{34}$$

In Equation (34), δ_{PG} is the size of the infiltration flow distance and $\dot{m}_{PG}$ is the conductivity coefficient of the infiltration flow distance. By solving the above equations and calculating the values of $\dot{q}_{PG}$, J_p, T_{Mp}, T_{PG}, T_{Me}, T_{Co}, T_{Eo}, it can be written:

$$\dot{m}_{Eo} = \dot{m}_{Ei} - \dot{m}_{PG} = \dot{m}_{Ei} - J_p A_M \tag{35}$$

$$S_{Eo} = \frac{\dot{m}_{Ei} S_{Ei}}{\dot{m}_{Eo}} \tag{36}$$

In the equations above, $\dot{m}_{Eo}$, $\dot{m}_{PG}$ are the mass rates of fluid at the outlet of the evaporator and the total mass rate of infiltrating freshwater in the distance of the infiltrating flow, respectively. Also, A_M is the area of the membrane. S_{Eo}, and S_{Ei} are the water salinity at the inlet and outlet of the evaporator channel, respectively.

2.5.2. Exergy Equations

The exergy of the saltwater mixture is obtained from the following equations [16]:

$$EX = (h - h^*) - T_0(s - s^*) + mf_s \left(\mu^0 - \mu^* \right) + mf_W \left(\mu^0 - \mu^* \right) \tag{37}$$

$$EX_{dist} = (m_{in,k} EX_{in,k}) - (m_{out,k} EX_{out,k}) + \left((Q_{loss}) \left(1 - \frac{T_o}{T_{e-c}} \right) \right) \tag{38}$$

3. Results

3.1. Concentration Photovoltaic/Thermal System

The results on the amount of electricity produced, the amount of electricity consumed and the amount of useful electrical energy are shown on a monthly basis in Figure 6. As can be seen, the amount of electricity produced varies between 4 and 9 megawatt hours per month. The amount of thermal exergy, exergy of lost heat and exergy of useful heat are shown on a monthly basis in Figure 7. As can be seen, the amount of monthly heat exergy varies between 2.6 to 3.8 MWh and the amount of useful heat exergy varies between 4 to 6.9 MWh.
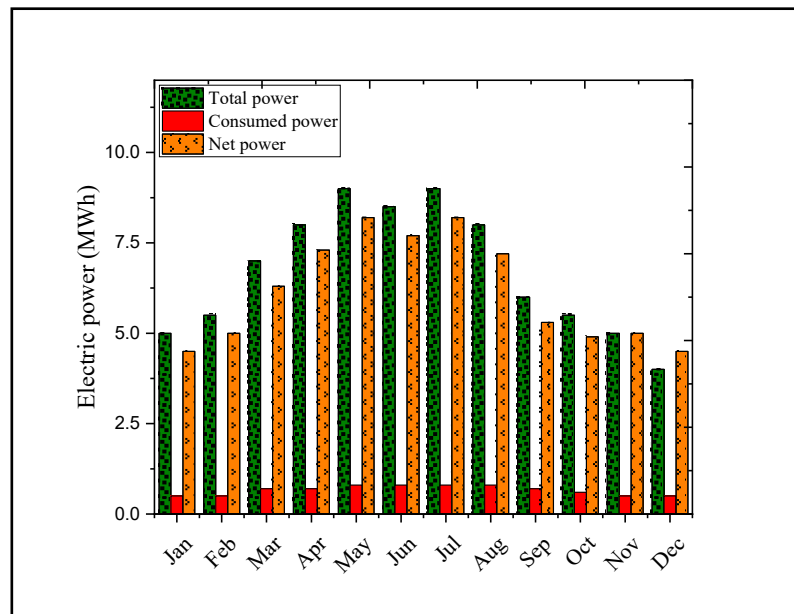
Figure 6. The amount of electricity produced, the amount of electricity consumed and the amount of monthly useful electrical energy in the city of Kerman.
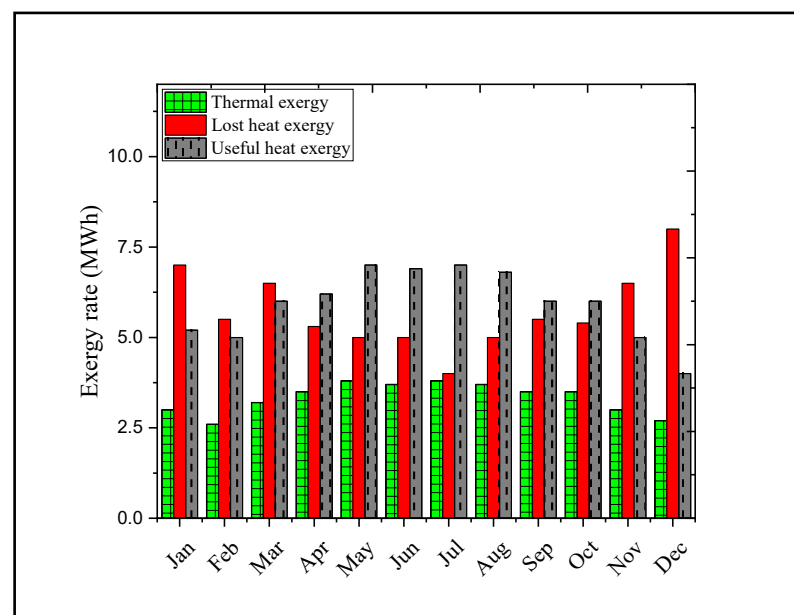

Figure 7. Thermal exergy, lost heat exergy and monthly useful heat exergy in Kerman city.

3.2. Organic Rankine Cycle

In Figure 8, the amount of exergy of the incoming flow (fuel exergy), exergy of the outgoing flow (product exergy) and destroyed exergy are shown for the months of the year.

According to the figure, the highest amount of monthly exergy of the incoming flow is 5.1 MWh in May and the lowest monthly exergy of the incoming flow is 3.28 MWh in February, also the highest amount of destroyed monthly exergy is 1.41 MWh in May and the lowest amount of destroyed monthly exergy is 0.79 MWh. In Figure 9, the exergy level of the Sigel single-effect lithium-bromide absorption cooling components are shown for the months of the year.
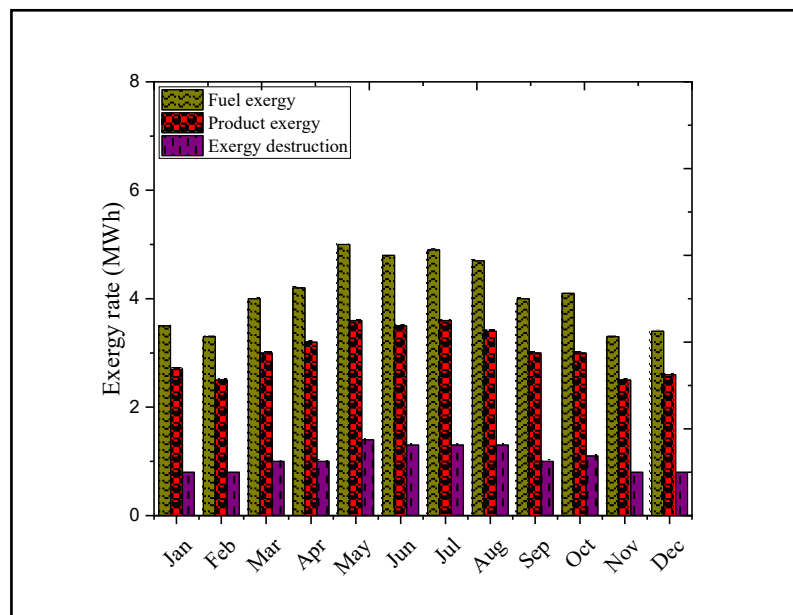
Figure 8. Amount of exergy of the incoming flow, exergy of the outgoing flow and destroyed exergy for the months of the year.
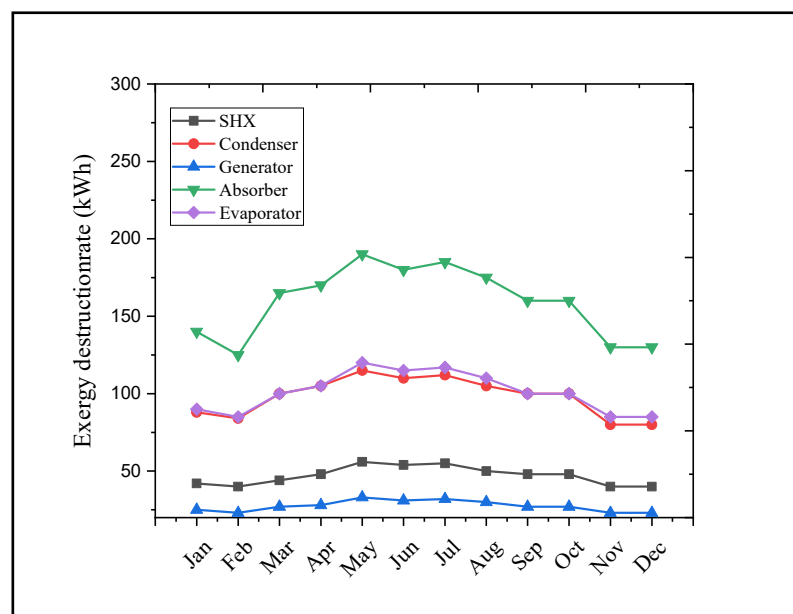

Figure 9. The exergy level of the Sigel single-effect lithium-bromide absorption cooling components for the months of the year.

According to the figure, the monthly exergy amount of the heat exchanger changes from 22.9 to 190.1 kWh, which is the highest in May and the lowest in November and December. Also, the average monthly exergy of the generator is 22.9 and 33.2 kWh, respectively. In addition, the amount of monthly exergy of the evaporator changes from 85 to 120 kWh and the amount of monthly exergy of the condenser changes from 80.2 to 115.50 kWh.

3.3. Desalination System

In Figure 10, the amount of freshwater produced and the heat taken by the desalination plant are shown for the months of the year.
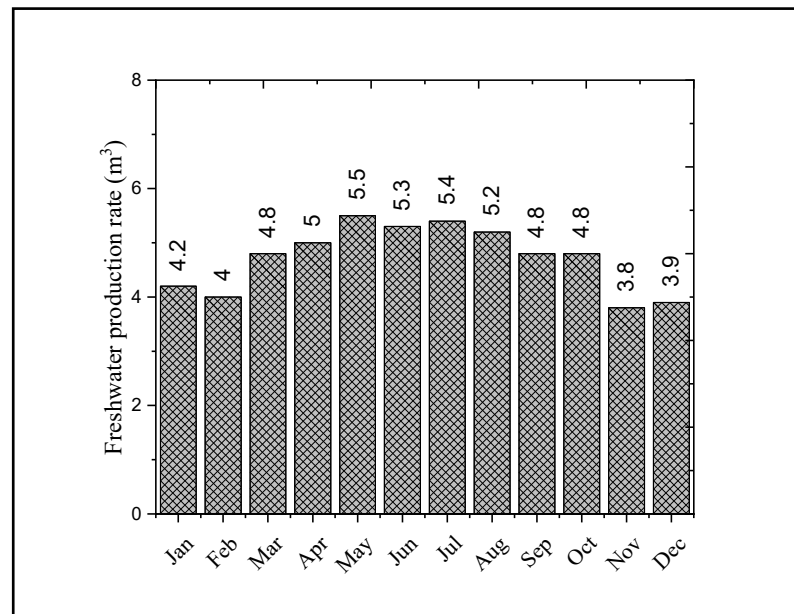
Figure 10. The amount of freshwater produced and the heat taken by the desalination plant for the months of the year.

According to the figure, the freshwater production rate of the desalination plant is approximately 56.7 m^3/year; the lowest was 3.8 m^3 in November. Obviously, in the months when high solar radiation is available, higher thermal energy can be fed into the desalination unit to produce freshwater.

In Figure 11, the amount of total exergy, evaporator exergy and condenser exergy are shown for the months of the year.
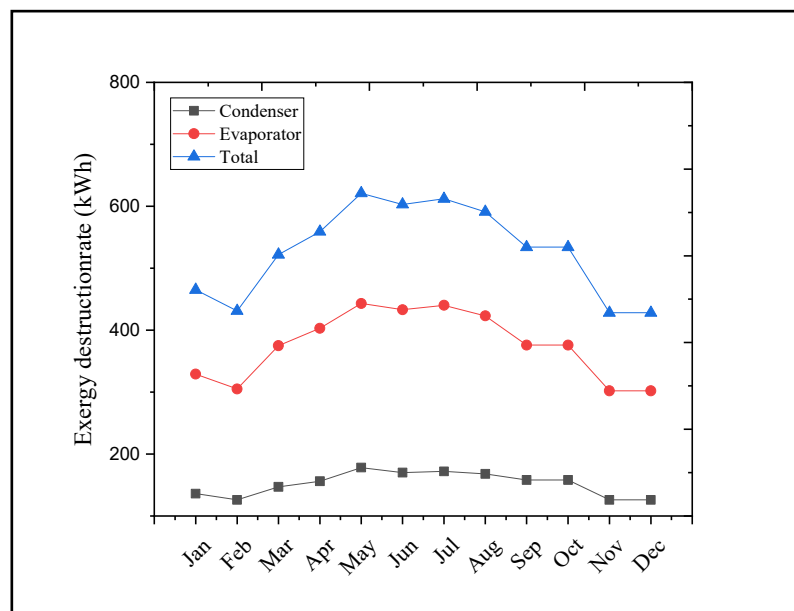
Figure 11. Total exergy, evaporator exergy and condenser exergy for the months of the year.

According to the figure, the monthly exergy amount of the condenser changes from 125.8 to 178 kWh, which is the highest in May and the lowest in February, and its monthly average is 151.8 kWh. Energy systems based on solar technologies basically have a high exergy destruction rate, because a small share of incoming solar energy can be converted into useful energy (electricity and/or heat). According to the literature (Ma et al. 2022) [17],

in solar energy-driven systems, the rate of exergy destruction can increase with the increase of solar radiation. For this reason, in the months of the year when solar radiation is higher than other months, the exergy destruction rates of the components as well as the overall exergy destruction rate are higher (see Figures 9 and 11).

4. Conclusions

In this study, a combined thermal concentrator photovoltaic system, organic Rankine power generation cycle, water/lithium and bromide absorption cooling system and membrane distillation desalination system were investigated. The useful electrical energy of the combined photovoltaic system is 76.74 MWh. In the organic Rankine power generation cycle, the annual exergy rate of the incoming stream is 48 MWh, the annual production exergy rate is 54.4 MWh and the annual destroyed exergy rate is 43.1 MWh. Moreover, the annual energy yield of the cycle is 65.10% and the annual exergy yield is 95.52%. In the absorption refrigeration cycle, the efficiency of the cycle is 72% and its exergy efficiency is 57.17%. The amount of heat taken by the water desalination in the year is 52.62 MWh and also the amount of destroyed exergy of the evaporator is 49.4 MWh, the condenser is 1.83 MWh and also the amount of destroyed exergy is 32.6 MWh. The amount of freshwater produced in the year is 56.7 m^3, the output ratio is 41.3 and the recovery ratio is 57.2. In general, for the combined system, thermal efficiency and exergy efficiency has been obtained, 75% and 93.72%, respectively.

Author Contributions: Conceptualization, A.A.A.A., M.I.A., I.H.A.-K. and R.A.; methodology, A.C., M.S.K., I.H.A.-K. and R.A.; software, A.A.A.A., M.I.A. and A.C.; validation, A.A.A.A., M.I.A., A.C., M.S.K. and R.A.; formal analysis, I.H.A.-K. and R.A.; investigation, A.A.A.A., M.I.A., A.C., M.S.K., I.H.A.-K. and R.A.; resources, A.A.A.A., M.I.A., A.C. and M.S.K.; data curation, A.A.A.A., A.C., M.S.K. and R.A.; writing—original draft preparation, A.A.A.A., M.I.A., M.S.K., I.H.A.-K. and R.A.; writing—review and editing, A.C., M.S.K., I.H.A.-K. and R.A.; visualization, A.A.A.A., M.I.A., A.C. and M.S.K.; supervision, R.A.; project administration, R.A. All authors have read and agreed to the published version of the manuscript.

Data Availability Statement: All data used to support the findings of this study are included in the article.

Conflicts of Interest: The authors declare no conflict of interest.

Nomenclature

A	Area (m^2)
a	Temperature coefficient
C	Concentration ratio
EX	Exergy rate (kW)
e	Specific exergy
F	Fill factor
h	Specific enthalpy (kJ/kg)
I_{bT}	Direct solar radiation (W/m^2)
J_P	Mass transfer rate
k_m	Conductivity coefficient
$\dot{m}$	Mass flow rate (kg/s)
n	Cells number
P	Power (kW)
$\dot{Q}$	Heat transfer rate (kW)
s	Specific entropy (kJ/kg·K)
T	Temperature (°C)
$\dot{W}$	Work (kW)
X	Solution concentration ratio

Greek symbols

δ_m	Membrane thickness
η	Thermal efficiency (%)
ψ	Exergy efficiency (%)

Subscripts

a	ambient
abs	absorber
c	cell
coll	collector
con	condenser
ev	evaporator
gen	generator
id	ideal
in	inlet
opt	optical
out	outlet
par	parasitic loss
sol	solar
T	turbine

Abbreviations

ARS	Absorption refrigeration system
COP	Coefficient of performance
CPV/T	Concentrator photovoltaic/thermal
EES	Engineering equation solver
MD	Membrane desalination
ORC	Organic Rankine cycle
PTC	Parabolic trough collector
SF	Solar fraction
TF	Thermal factor

References

1. Moltames, R.; Roshandel, R. Techno-economic analysis of a modified concentrating photovoltaic/organic Rankine cycle system. *Int. J. Ambient. Energy* **2022**, *43*, 2026–2038. [CrossRef]
2. Rahbar, K.; Riasi, A.; Sangjoeei, H.K.B.; Razmjoo, N. Heat recovery of nano-fluid based concentrating Photovoltaic Thermal (CPV/T) Collector with Organic Rankine Cycle. *Energy Convers. Manag.* **2019**, *179*, 373–396. [CrossRef]
3. Albaik, I.; Alamri, Y.A.; Elsheniti, M.B.; Al-Dadah, R.; Mahmoud, S.; Ismail, M.A. Assessment of a novel multi-generation solar CPV/T system combining adsorption and organic rankine cycle subsystems. *Sol. Energy* **2022**, *236*, 455–472. [CrossRef]
4. Noorollahi, Y.; Yousefi, H.; Moltames, R.; Choubineh, K. Techno-economic Performance Analysis of a Hybrid Concentrated Photovoltaic/Thermal Combined with Organic Rankine Cycle (CPV/T-ORC) system for Simultaneous Generation of Power and Heat. *J. Renew. New Energy* **2022**, *9*, 113–120.
5. Elminshawy, N.A.; Gadalla, M.A.; Bassyouni, M.; El-Nahhas, K.; Elminshawy, A.; Elhenawy, Y. A novel concentrated photovoltaic-driven membrane distillation hybrid system for the simultaneous production of electricity and potable water. *Renew. Energy* **2020**, *162*, 802–817. [CrossRef]
6. Heng, Z.; Feipeng, C.; Yang, L.; Haiping, C.; Kai, L.; Boran, Y. The performance analysis of a LCPV/T assisted absorption refrigeration system. *Renew. Energy* **2019**, *143*, 1852–1864.
7. Buonomano, A.; Calise, F.; Palombo, A. Solar heating and cooling systems by absorption and adsorption chillers driven by stationary and concentrating photovoltaic/thermal solar collectors: Modelling and simulation. *Renew. Sustain. Energy Rev.* **2018**, *82*, 1874–1908. [CrossRef]
8. Rabiea, M.; Ali, A.Y.; Abo-Zahhad, E.M.; Elqady, H.I.; Elkady, M.F.; Ookawar, S.; El-Shazly, A.H.; Salem, M.S.; Radwan, A. Thermal analysis of a hybrid high concentrator photovoltaic/membrane distillation system for isolated coastal regions. *Sol. Energy* **2021**, *215*, 220–239. [CrossRef]
9. Moaleman, A.; Kasaeianb, A.; Aramesh, M.; Ahian, O.; Sahota, L.; Tiwari, G.N. Simulation of the performance of a solar concentrating photovoltaic-thermal collector, applied in a combined cooling heating and power generation system. *Energy Convers. Manag.* **2018**, *160*, 191–208. [CrossRef]
10. Flamant, G. Solar Power Plants: State of the Art. In *Concentrating Solar Thermal Energy: Fundamentals and Applications*; Wiley: Hoboken, NJ, USA, 2022; p. 1.
11. Al-Nimr, M.A.; Dawahdeh, A.I.; Al-Omari, J.A. Dual power generation modes for thermally regenerative electrochemical cycle integrated with concentrated thermal photovoltaic and phase change material storage. *J. Energy Storage* **2023**, *58*, 106373. [CrossRef]

12. Indira, S.S.; Vaithilingam, C.A.; Narasingamurthi, K.; Sivasubramanian, R.; Chong, K.K.; Saidur, R. Mathematical modelling, performance evaluation and exergy analysis of a hybrid photovoltaic/thermal-solar thermoelectric system integrated with compound parabolic concentrator and parabolic trough concentrator. *Appl. Energy* **2022**, *320*, 119294. [CrossRef]

13. Wang, Z.; Xie, B.; Xia, X.; Yang, H.; Zuo, Q.; Liu, Z. Energy loss of radial inflow turbine for organic Rankine cycle using mixture based on entropy production method. *Energy* **2022**, *245*, 123312. [CrossRef]

14. Mohammadi, S.H. Theoretical investigation on performance improvement of a low-temperature transcritical carbon dioxide compression refrigeration system by means of an absorption chiller after-cooler. *Appl. Therm. Eng.* **2018**, *138*, 264–279. [CrossRef]

15. Mahmoudi, G.; Goodarzi, M.; Dehghani, S.; Akbarzadeh, A. Experimental and theoretical study of a lab scale permeate gap membrane distillation setup for desalination. *Desalination* **2017**, *419*, 197–210. [CrossRef]

16. Najib, A.; Orfi, J.; Ali, E.; Saleh, J. Thermodynamics analysis of a direct contact membrane distillation with/without heat recovery based on experimental data. *Desalination* **2019**, *466*, 52–67. [CrossRef]

17. Ma, L.; Mao, J.; Marefati, M. Assessment of a new coal-fired power plant integrated with solid oxide fuel cell and parabolic trough solar collector. *Process Saf. Environ. Prot.* **2022**, *163*, 340–352. [CrossRef]